RSC Advances

ROYAL SOCIETY OF CHEMISTRY

www.rsc.org/advances

Journal Name

ARTICLE

Visible-light-driven floriated $ZnIn_2S_4/AgIn_5S_8$ heteromicrospheres catalyst for dye degradation

Received 00th January 20xx,
Accepted 00th January 20xx

DOI: 10.1039/x0xx00000x

www.rsc.org/

Jiangluqi Song,[a] Tongtong Jiang,[a] Gengwu Ji,[b] Wenting Zhang,[a] Xiangyi Cheng,[a] Wei Weng,[a] Lixin Zhu*,[c] Xiaoliang Xu*,[a]

We report the synthesis of $ZnIn_2S_4/AgIn_5S_8$ (ZIS/AIS) heteromicrospheres with tailorable composition and controllable band gap via partial cation exchange for the first time. Detailed studies of the as-prepared samples were carried out by SEM, TEM, STEM-EDS, XRD and layer-by-layer depth XPS analysis. Based on these results, a possible cation exchange was proposed, and a critical concentration of Ag^+ in crystals was identified below which cation exchange cannot occur. Besides, enhanced photodegradation mechanism was discussed by analyzing the UV-vis-NIR reflectance spectra and the band structure, illustrating that a proper thickness of AIS layer is beneficial to the generation of active species thus favors the degradation reaction. Further application of dye degradation demonstrated a remarkable photodegradation rate up to 99.2%. Our result shed light on how the cation exchanged happened between ternary and binary crystals, which may open a new avenue to the field of synthesizing materials at the micro-scale.

1. Introduction

Ternary semiconductors, such as Ag-In-S (AIS) and Cu-In-S, contains "non- Class A metal", has gained intensive attention in biolabeling, opto-electronic devices and solar cell for its wonderful biocompatibility, nice defect tolerance and excellent optical properties.[1-10] Among them, $ZnIn_2S_4$ (ZIS)semiconductor, have attracted considerable interest in light emitting diodes and photocatalysis because of its lower cost and more convenient approach than that of I-III-VI materials.[1, 7, 11-21] However, ZIS semiconductor, didn't exhibit an admirable light utilization efficiency than AIS (band gap 1.8-2.1 eV) material in photocatalysis and solar cells because of their relatively wide band gap (2.4-2.8 eV).22, 23 Apparently, exploration of new strategies for producing materials with the comprehensive advantages of these two kinds of semiconductors is still expected.

In the field of material synthesis, meanwhile, of particular interest is the cation exchange method which can preserve the pristine crystal frameworks, playing a significant role for producing materials of diverse shapes and desired composition.[1, 4, 24-31] Giving the obvious merits, a series of achievements have been made during the recent years. Son and his co-workers[30] found that the shapes of obtained nanocrystals was pronounced influenced by their critical size during the cation exchange process. Akkerman et al.[1] realized the transformation from binary nanocrystals to ternary and quaternary nanocrystals by adjusting the exchange sequence. Miszta et al.[25] presented an example of a nanostructure in which branching structure was achieved by proper organization of different domains in a single nanocrystals. Van der Stam's[32] group has prepared luminescent $CuInS_2$ quantum dots starting from Cu-S binary nanocrystals. Yet, no research of cation exchange reaction at the micro-scale in aqueous system has been reported. In addition, there still exist a crucial question that how exactly the cations in the initial crystal are replaced by the guest cations.

In this paper, cubic $ZnIn_2S_4/AgIn_5S_8$ (ZIS/AIS) hetero-microspheres (HMSs) with visible light absorption were successfully synthesized via partial cation exchange. A possible mechanism of cation exchange was proposed on the basis of XRD and XPS depth measurements, according to which pure AIS and Ag_2S MSs were also prepared. By analyzing the optical absorption, the band structure of ZIS/AIS HMSs was obtained and the mechanism enhanced photodegradation was discussed. What' more, visible light driven degradation test of dye was performed, showing a high photodegradation rate up to 99.2%. Our work would demonstrate that, in place of doping method, cation exchange could be used as a facile and versatile approach for synthesis of band controllable and composition tailorable ZIS/AIS heterostructure which have potential application in solar cell and hydrogen evolution.

[a]Key Laboratory of Strongly-Coupled Quantum Matter Physics, Chinese Academy of Sciences, and Department of Physics, University of Science and Technology of China, Hefei, Anhui 230026, China

[b]Shanghai Institute of Applied Physics, Chinese Academy of Sciences, Shanghai, 201204, China.

[c]Center Laboratory, First Affiliated Hospital of Anhui Medical University, Hefei 230026, China

Electronic Supplementary Information (ESI) available: SEM images of broken ZIS MSs and AIS catalyst. STEM-EDS line scan of sample H1, SEM, HRTEM, XRD and method of prepared AIS and Ag_2S MSs. See DOI: 10.1039/x0xx00000x

2. Experimental Section

2.1 Chemicals.

Zinc nitrate hexahydrate ($Zn(NO_3)_2•6H_2O$, 99.99%), silver nitrate ($AgNO_3$, 99.99%), thioacetamide (TAA, 99%), nitric acid, methanol, and absolute ethanol were purchased from Sinopharm Chemical Reagent Co. Ltd. (Shanghai, China). Indium acetate ($In(OAc)_3$, 99.99%) was purchased from Alfa Aesar Chemical Reagent Co. (China). All chemicals are of analytical grade and used as received without further purification. All the water used in experiments was deoxidized deionized water (18.25 MΩ•cm).

2.2 Synthesis of floriated ZIS microspheres.

Floriated ZIS microspheres were synthesized via a hydrothermal process according to the previous report with large modifications.[15, 33] Typically, 2 mmol of $Zn(NO_3)_2•6H_2O$, 4 mmol of $In(OAc)_3•4.5H_2O$, and 10 mmol of thioacetamide (TAA) were dissolved in 30 mL of water. Then, 1 M nitric acid was introduced so that pH=2 was achieved. Subsequently, the mixture was sealed in a Teflon-lined stainless steel autoclave, and heated to 90 °C with a heating rate of 5 °C/min and kept at this temperature for 4 h. After naturally cooled to room temperature, the orange precipitates were washed with water and ethanol alternately and dried at 70 °C for further use. The Ag-In-S microspheres were synthesized similarly except that the amount of $AgNO_3$ was 1 mmol.

2.3 In situ Cation Exchange preparation of ZIS/AIS heteromicrospheres (HMSs).

A certain amount of $AgNO_3$, and 0.001 mmol of $In(OAc)_3•4.5H_2O$ were dissolved in 10 mL water, and added into 20 mL water which contain 1 mmol of previously synthesized ZIS MSs and 800 µL of methanol. Then the mixture was transferred into an autoclave and kept at 90 °C for 3 h. Then the temperature was raised to 150 °C and kept for another 3 h. The purification and drying of ZIS/AIS HSMSs were the same as that of ZIS MSs. In this work, we set the molar ratio of Ag to Zn (total Zn in the ZIS MSs) as 0.5, 0.75, 1 and 1.25, noting as H1-H4.

2.4 Material characterization

The transmission electron microscopy (TEM) and high resolution transmission electron microscopy (HRTEM) images were measured by JEOL JEM 1400 working at 200 kV. The elemental line profile were performed on a JEOL JEM-2100F equipped with a field emission gun working at 200 kV. The general morphology of the samples was investigated with scanning electron microscopy (SEM, JEOL JSM 6700F) equipped with an energy dispersive X-ray spectrometer (EDX) attachment. The elemental contents of samples were detected by using a Shimadzu X-ray fluorescence (XRF) spectrometer (XRF 1800). XRD measurements were conducted on a MXPAHF 18 kW diffractometer with Cu Kα (0.154 nm) serving as the incident radiation. The samples were pre-prepared by thorough grinding and drying. The UV-vis diffuse reflectance spectra (DRS) were acquired by a Shimadzu Solid 3700 UV-vis-NIR spectrophotometer equipped with an integrating sphere. The Brunauer−Emmett−Teller (BET) surface area was measured with an ASAP2010 M apparatus. All the samples were degassed at 120 °C overnight prior to BET measurements. The nitrogen adsorption and desorption isotherms were measured at −196 °C.

2.5 X-ray Photoelectron Spectroscopy (XPS) depth profiles

XPS was measured by Phoibos 100 analyzer with pass energy 10eV which was calibrated by Fermi level (EF) of Au. Standard Al Kα (1486.61 eV) composed of a monochromator was used as x-ray source with a base ultrahigh vacuum of 10-10 mbar. The resolution of XPS was 0.6 eV measured as a full width at half maximum (FWHM) of Ag 3d5/2 peak with the pass energy of 10 eV. The depth profile analysis were performed by bombarding the surface of the samples with Ar+ ions accelerated at a high voltage of 1.5 kV with the sample current of 1.5 µA. The sputtering rate of the samples was about 1 nm/min under these pre-set conditions, and data were collected at an interval of 5 min. All the spectra were corrected by C 1s peak at 285.0 eV. Quantitative elemental compositions were measured from peak areas using experimentally determined sensitivity factors and the spectrometer transmission function. The high-resolution spectra were deconvoluted to Gaussian−Lorentzian function by means of the Casaxps software.

2.6 Photocatalystic degradation of dye.

Rhodamine B (RhB) was used to evaluate the photodegradation performance of the prepared MSs and HMSs. The standard absorption curve was calibrated by measuring the absorbance of various concentration of Rhodamine B solution at 554 nm. 30 mg of photocatalyst, i.e. ZIS MSS and ZIS/AIS HMSs (sample H1-H4), were respectively suspended in 100 mL solution containing 60 ppm of RhB. Prior to irradiation, the suspension was magnetically stirred in the dark environment to ensure the establishment of an adsorption-desorption equilibrium. At a given interval, a small amount of the suspension was taken out, centrifuged, and the supernate was analysed by UV-vis spectrophotometer. After the pre-adsorption (PA), a 500 W tungsten halogen lamp equipped with a cutoff filter that can remove wavelength less than 420 nm was served as visible light source. To monitor the degradation, aliquots of the sample were taken out at different time intervals to examine their absorption spectra (ditto). The rate of photodegradation was calculated use the equation, $R=(C_0-C)\times100\%/C_0$, where R, C_0 and C represent the degradation rate, initial concentration and the current concentration of different interval, respectively.

3. RESULTS AND DISCUSSION

3.1 Morphology and crystal structure

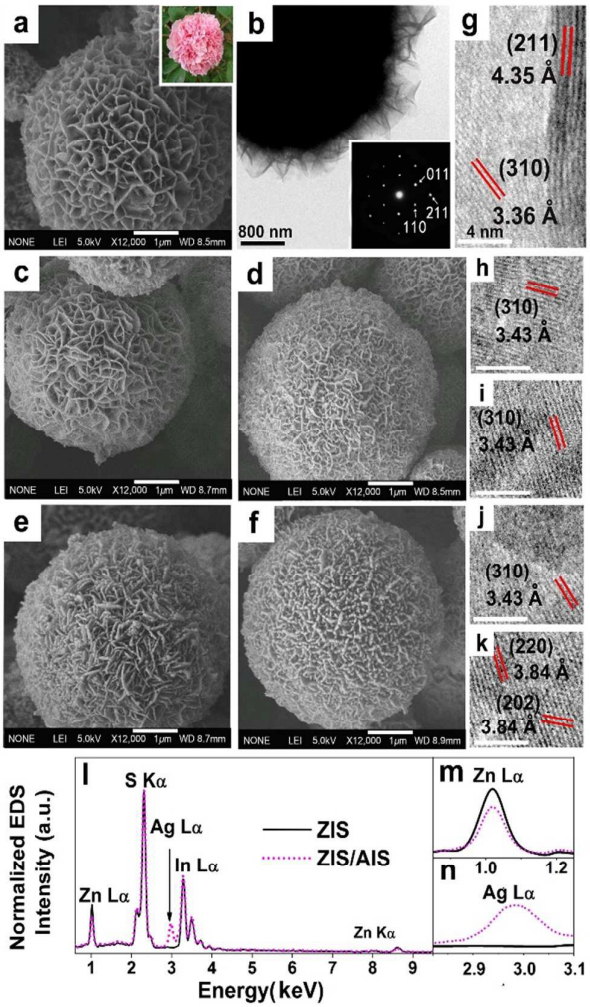

Figure 1. SEM images of (a) initial ZIS MSs and (c-f) the HMSs for sample H1-H4 (inset of (a): photograph of a real peony flower). (b) TEM image of initial ZIS MSs (inset: corresponding Fourier transform). (g-k) HRTEM characterization of above corresponding samples. The EDS of the (l) pristine ZIS MSs and ZIS/AIS HMSs H1, and their evolution of (m) Zn Lα and (n) Ag Lα spectra. (scale bar: 4 nm)

Figure 1a is the representative SEM image of initial ZIS MSs. It shows that the product is a solid sphere, which can be deduced from some broken parts (shown in Figure S1), just like a peony, with an average diameter of 5 μm. The surface composed of plenty of nanosheets/nanoflakes, which is more homogeneous than the previous reported.[33] The flaky mesoporous structure may make for photocatalytic reaction because of the large specific surface area. Figure 1c-1f are the SEM images of ZIS/AIS HMSs prepared *in situ* by cation exchange reaction under the same experimental condition with different molar ratio of the reaction precursors of Ag to

Table 1. Element content analysis of ZIS MSs and ZIS/AIS

sample	Zn/wt.%	Ag/wt.%	In/wt.%	S/wt.%	composition
ZIS	14.74	--	55.06	30.20	$ZnIn_{2.13}S_{4.19}$
H1	13.03	2.64	54.46	29.86	$Zn_{0.9}Ag_{0.11}In_{2.13}S_{4.19}$
H2	11.90	5.00	53.70	29.44	$Zn_{0.83}Ag_{0.21}In_{2.12}S_{4.17}$
H3	11.00	6.64	52.97	29.39	$Zn_{0.77}Ag_{0.28}In_{2.10}S_{4.18}$
H4	9.91	7.87	52.79	29.43	$Zn_{0.69}Ag_{0.33}In_{2.08}S_{4.16}$

ZIS of 0.5, 0.75, 1.1 and 1.25, noted as sample H1-H4. It reveals that, different with the doping method[15] and compared with directly synthesized AIS catalyst by hydrothermal protocol (Figure S2), the HMSs respectably preserved the flake-like and porous structure, except for some slightly crimps on the edge of the nanosheets (Figure 1d and 1e). This may be the result of a distortion caused by the mismatch between AIS and ZIS crystal in the surface region of the nanosheets. Lots of nanosheets are clearly seen on the surface of the MSs from the TEM image (Figure 1f). Figure 1g is HRTEM image of a nanosheet belong to a pristine ZIS microsphere, showing the (211) and (310) lattice sets of cubic $ZnIn_2S_4$ with the interplanar spacings of 4.35 and 3.36 Å, respectively. Besides, the HRTEM images of H1-H4 also show the (310), (220) and (202) lattice sets of cubic $AgIn_5S_8$, indicating the formation of AIS components. Normalized by the intensity of S peak, EDX spectrum (Figure 1l) shows the characteristic peaks of Zn Lα, In Lα and S Kα of ZIS MSs with an intensity about 1:2:4, consisting with the stoichiometric form of $ZnIn_2S_4$, and an Ag Lα peak of ZIS/AIS HMSs. The magnified spectra of Zn Lα and Ag Lα shown in Figure 1m and 1n demonstrates that there is a decrease of Zn content and an emergence of Ag content respectively, which qualitatively clarified the reaction of cation exchange of Zn^{2+} to Ag^{+}.

It is noteworthy that the In contents seems remained elementary invariant, which were also seen in other cation reaction of Zn to $AgInS_2$[4] and Zn to $CuInS_2$[34]. Confirmed by XRF measurement as shown in Table 1, there is a continuous decrease of Zn content accompanies with an increase of Ag, while In content stays nearly constant. Because of the smaller radius of Zn^{2+} (0.74 Å) which suffers weaker potential barrier in migration than In^{3+} (0.81 Å) in lattice,[5, 35] it is conceivable that Zn^{2+} has the priority to exchange with Ag^{+}. However, we consider this not enough believable. If this is the case, Ag^{+} which has a larger radius (1.26 Å) can hardly enter the ZIS lattice,[36, 37] let alone to exchange with Zn^{2+}. A more likely explanation arises when we considered the configuration of atoms in cubic X-In-S (X stand for Ag, Cu or Zn). Unit cell structure diagram of cubic $ZnIn_2S_4$ shows (Scheme 1) that each In atom is bonded to six nearest S atoms, yet there are four S atoms around a Zn atom. As a result, In possesses a more stable chemical state than Zn, and they can difficultly exchange with surrounding cations, such as Ag^{+}, Cu^{+} and Zn^{2+}.

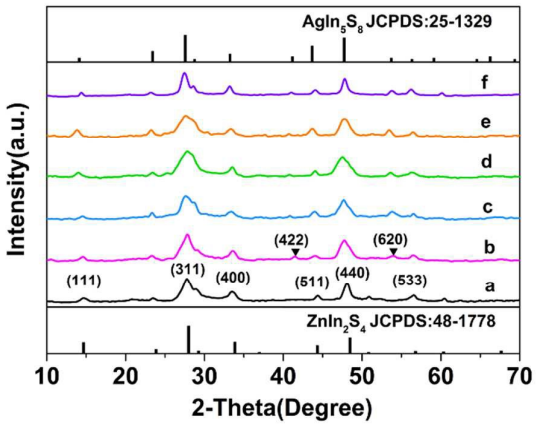

Figure 2. XRD patterns of pristine ZIS MSs (a), sample H1-H4 (b-e) and pure $AgIn_5S_8$ (f) derived from cation exchange (▼ indicate the peaks of cubic AIS phase).

The phase and crystallographic structure of the products were determined by XRD. Figure 2 shows that all the diffraction peaks of the initial ZIS MSs could be indexed to a cubic phase of $ZnIn_2S_4$ (JCPDS No.48-1778, a=10.621 Å)[11], and no other impurities such as In_2S_3 or ZnS are found. Similarly, the profiles of the ZIS/AIS HMSs samples are same as the cubic $ZnIn_2S_4$, except for the appearance of (422) and (620) diffraction peak of cubic $AgIn_5S_8$ (JCPDS No.25-1329, a=10.825 Å)[34]. It doesn't seem strange that the whole XRD patterns exhibit the same crystalline phase, for the reason that the anion sublattice, i.e. S^{2-} subframes, maintained their structural rigidity and shape during the exchange reaction.[23,28,35] Because of the similar ternary composition, and the same bonding situation and the identical atomic sites between $AgIn_5S_8$ and $ZnIn_2S_4$, the position of diffraction peaks hold almost the same lines. Nevertheless, the interplanar spacing (a=10.825 Å of cubic $AgIn_5S_8$) has a tiny distinction on account of the different ions radius between Zn^{2+} and Ag^+ which resulted in the shift of the peaks. So as a consequence, there is a broadening of (311) and (440) diffraction peaks in the profiles of sample H2-H4. Due to the relatively large size of the HMSs and the uneven surface, the STEM-EDS curves don't show clear and accurate elemental distribution of as-prepared HMSs, except for a roughly estimated thickness of 70 nm for AIS region (sample H1) (shown in Supporting information Figure S3).

3.2 Influence of Experimental Conditions

ZIS MSs were synthesized by template-free hydrothermal protocols in the absence of templates or surface ligands. According to the acid-base theory, as a soft base, S^{2-} can easily react with Zn^{2+} and In^{3+}, which are Lewis base, to form a stable product, and self-assemble to a microsphere with irregular nanosheets. Previous study shows that the reaction temperature and pH value have a significant effect on the size and morphology of ZIS MSs.[10] Here in this paper, as the ZIS/AIS HMSs were prepared *via* cation exchange method for the first time, we only focus on the influence of the composition on the reaction temperature and concentration of Ag^+ precursor in sample H1 during the exchange precess, where we immobilized all the other experimental variables as set in the Experimental Section.

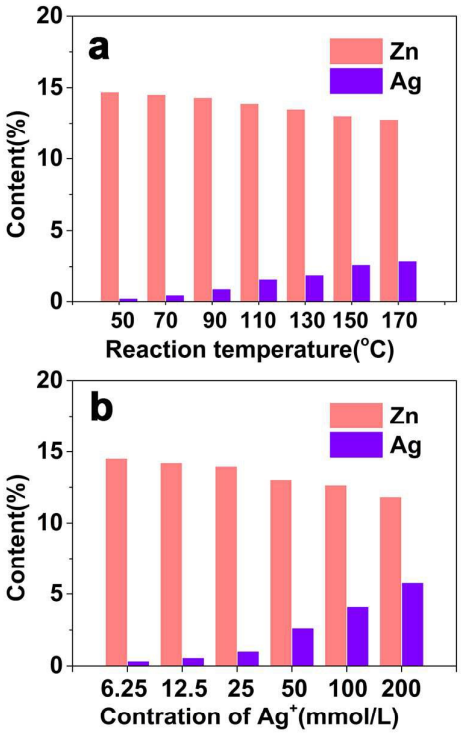

Figure 3. Dependence of Zn and Ag content upon different (a) reaction temperature and (b) concentration of Ag^+.

3.2.1 Effect of reaction temperature. The composition of the HMSs was pronouncedly influenced by the reaction temperature as is seen in Figure. With the raise of the reaction temperature, Ag^+ content increase accompany with the reduction of Zn^{2+}, showing that Ag^+ was more easily exchanged by Zn^{2+} at a higher temperature. It is reported that thermal defects, such as Frenkel defect, dominate the whole exchange process.[22] That is, the propagation of the cations, i.e. Ag^+ and Zn^{2+}, was performed by hopping in the vacancies of cations. With the enhancement of the temperature, the concentration of the vacancies which is equal to $2\exp(-\Delta H_{Frenkel}/2kT)$ ($\Delta H_{Frenkel}$ is the formation enthalpy of Frenkel defect) increased accordingly, and thus the amount of exchange cations augmented.

3.2.2 Effect of Ag+ concentration. The content of Zn and Ag were found to be strongly depended on the concentration of Ag^+ precursor. Under concentration of 25 mmol/L of Ag^+, the content of Zn stayed constant while Ag increased, which demonstrate the incorporation of Ag^+ into the ZIS MSs without cation exchange. When the concentration of Ag^+ was above 25 mmol/L, the content of Zn was decreased. This phenomenon wasn't seen before, which cannot be explained by thermal defect for the number or the concentration of vacancies were identical under the same reaction temperature. This suggests

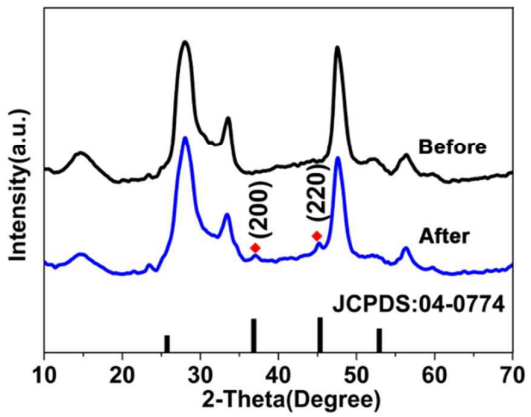

Figure 4. XRD patterns of ZIS MSs and ZIS MSs with the addition of $AgNO_3$ solution (◆indicate the peaks of cubic Ag_2S phase).

that the number or concentration of guest cations seems to be another factor which influences the exchange process which has not been reported yet, and will be discussed in the section of layer-by-layer XPS analysis.

During the experiment, we noticed a detail that a rapid color change (from orange to brown, <<1 s) of the ZIS MSs dispersion was observed upon adding excess amount of $AgNO_3$ without addition of $In(OAc)_3$ and heating. We investigated the XRD patterns of the samples before and after the addition of Ag precursor (shown in Figure 4). Not unexpectedly, two weak but evident diffraction peaks, which can be indexed to (200) and (220) crystal faces of cubic Ag_2S (JCPDS No. 04-0774, a=4.89 Å), are observed. This means that there were a tiny amount (about several layers) of Ag_2S formed on the very edge of the ZIS MSs and the cation exchange between Ag^+ and In^{3+} occurred, otherwise the X-ray diffraction phenomena wouldn't happen and the characteristic diffraction peaks wouldn't appear during the XRD measurement. This raises a question that how does the cation exchange process react, or whether the concentration of Ag^+ have an effect upon the aqueous exchange reaction in ternary semiconductor materials.

3.3 Layer-by-layer XPS profiles and cation exchange mechanism

To gain more information about the inertial layers and more conclusive mechanism of the cation exchange process in micrometer-sized ternary crystal, we performed layer-by-layer profile analysis of XPS on the samples acquired from different stage by Ar^+ sputtering. Figure 5a-5c are the XPS spectra derived from the ZIS MSs after adding $AgNO_3$ solution without heating. In accordance with XRD patterns (Figure 5b), the out layers (about several nanometers) are definitely Ag_2S with the atomic ratio of 2.3:1. The fitted two peaks with lower binding energy of Figure 5a are Ag 5d (374.7 eV for $3d_{3/2}$, 368.5 eV for $3d_{5/2}$) peaks, while the two satellites with higher binding energy are the oxidized states caused by the combination of

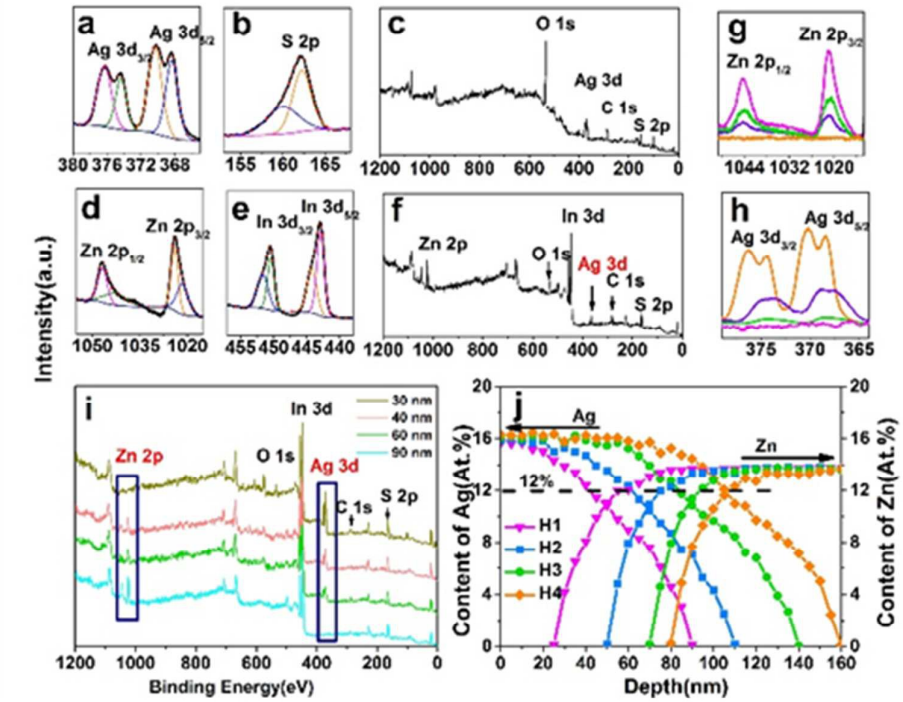

Figure 5. XPS profiles of (a) Ag 3d, (b) S 2p, (c) ZIS after adding in AgNO3 solution; (d) Zn2p, (e) In 3d, (f) ZIS MSs with sputtering 15 min ZIS after adding in AgNO3 solution; and high revolution spectra of (g) Zn 2p and (h) Ag 3d of (i) ZIS/AIS HMSs (sample H1) taken from different depth. And (j) contents of Ag and Zn derived from different depth of sample H1-H4.The black and red curves in Figure 5a, 5b, 5d and 5e respectively stand for the raw data and the fitting data.

Table.2 Element content analysis of ZIS MSs and products of control experiment

sample	content/wt.%				composition
	Zn	Ag	In	S	
original ZIS	14.74	--	55.06	30.20	$ZnIn_{2.13}S_{4.19}$
reaction A	13.79	4.87	52.2	28.71	$Zn_{0.98}Ag_{0.21}In_{2.13}S_{4.17}$
reaction B	12.07	5.21	53.46	29.26	$Zn_{0.84}Ag_{0.22}In_{2.12}S_{4.16}$

Table 3. Depth data of samples derived from XPS

sample	thickness of AIS/nm	thickness of ZAIS/nm	depth of reaction front/nm
H1	25	65	90
H2	50	60	110
H3	70	70	140
H4	80	80	160

the Ag with O during the synthesis. The two peaks of S 2p arise from the splitting of spin-orbital coupling.[36] Figure 5d-5f are the spectra taken after sputtering for 15 min of the above sample. It demonstrates that after stripping about 15 nm of outlayers, the stuff is Zn-In-S with the atomic ratio of 1:2.04:4.2 (identical to that of $ZnIn_2S_4$), while the two weak peaks of Ag 3d still exits. Previous studies manifested Ag^+ in cubic phase has a high diffusion coefficient similar to that in liquid (about 10^{-5} cm^2/s) which is influenced significantly by temperature.[28,32] So it can be inferred that because of the high mobility, Ag^+ can easily diffuse among the lattice of cubic $ZnIn_2S_4$, and doesn't have an impact on the structure and the composition of $ZnIn_2S_4$.

Further depth profile measurements were carried out to obtain more information about the components and contents of ZIS/AIS HMSs. Figure 5i is the XPS profile taken from different depth of representative sample H1. The spectrum of 30 nm depth shows a typical Ag-In-S curve without Zn, while material between 40-60 nm is gradient alloy of Ag-Zn-In-S (AZIS). The profile taken from the depth of 90 nm is the typical spectrum of $ZnIn_2S_4$. With the deepening of the sampling depth, the intensity of Ag 3d (Figure 5h) gradually decrease along with the increase of Zn 2p (Figure 5g) by degrees. Meanwhile, the oxidation satellites reasonably disappear while the position of Ag $3d_{3/2}$ and $3d_{5/2}$ stay unchanged, declaring the reduction of O in the inner microspheres.

Figure 5j shows plot of the contents for Ag and Zn which derived from different depth. The distribution of Ag content is in well agreement with the diffusion of Ag^+ in the cubic phase crystals.[37] Driven by the concentration gradient or chemical potential, the activated Ag^+ diffused in the interstice among S^{2-} sublattice,[32] which as a consequence, Ag content in sample H2 and H3 is higher than that in sample H1 and H2 in the surface segments, and gradually decreased in the diffusion direction. Zn didn't emerge in the initial 30 nm, revealing the formation of AIS composition. With the deepening of the detection, Zn increases progressively to a constant of 15.1%, which can be assigned to the content in $ZnIn_2S_4$. This clearly implies that cation exchange indeed exists inside the crystals. Groeneveld[22] and Shaw et al.[38] hold the viewpoint that the Frenkel defects dominant the whole exchange process that all the cation exchange occurs in the surface of the crystals, and subsequently both of the guest and native cation diffuse as interstitial among the lattice without exchange within crystals. They also insisted that temperature is the vital sensitive parameter during the cation exchange process thus strongly affects both the composition and the elemental distribution profile of the crystals. The most remarkable difference between organic and aqueous solution, however, seems to be the existence form of guest cations, namely, cations in organic solution must bond to organic ligands to form metal-ligand complex to stably exist, while in aqueous solution they are bare ions without any ligand which make them easier to incorporate into crystals and exchange with native cations. In this case, both XRD and XPS analysis clarifies that cation exchange can occur in interior of the materials.

Another information is found that Zn showed no distinct decrease until that the content of Ag was more than 12% (black imaginary line in Figure 3j), i.e. critical concentration, declaring that enough concentration of Ag^+ is the essential condition for the exchange reaction. In order to verify this point, another control experiment was carried out. We only change the way of the addition of Ag precursor, that is, Ag precursor of reaction A was added with a flow of 200 μL/min by a peristaltic pump, while Ag precursor of reaction B was put into the solution *via* a single injection, and the content and concentration of $AgNO_3$ and other conditions were identical. After reaction for 3 h, both of the two products were measured by XRF. Table 2 clearly demonstrates that products from continuous addition don't show a decrease of Zn content, while samples from a single injection obviously shows a reduction of Zn from 1 to 0.84 of the composition while the component of Ag is equally of both two sample. This result suggest that despite of the same content of Ag precursors, cation exchange of reaction A didn't occur because that the continuous added Ag^+ gradually diffused into the lattice of ZIS as uniform interstitials, just like doping, in which the concentration of Ag^+ couldn't reach the critical concentration, and Zn^{2+} couldn't be replaced by Ag^+ as a result. On the contrary, the single injection of Ag precursor ensured sufficient Ag^+ into ZIS, and cation exchange was accomplished.

So during the synthetic progress, a moderate temperature of 90 °C which can improve the activation energy of Ag^+, and thereby make for the incorporation and diffusion in ZIS MSs. Further heating (150 °C) can facilitate the exchange between Ag^+ and Zn^{2+} thus in favor of the reaction to our expected product. We define the diffusion depth of Ag^+ as reaction front, and the depth from the surface to the place where Zn

Scheme 1. Schematic diagram of cation exchange mechanism from ZIS to Ag_2S

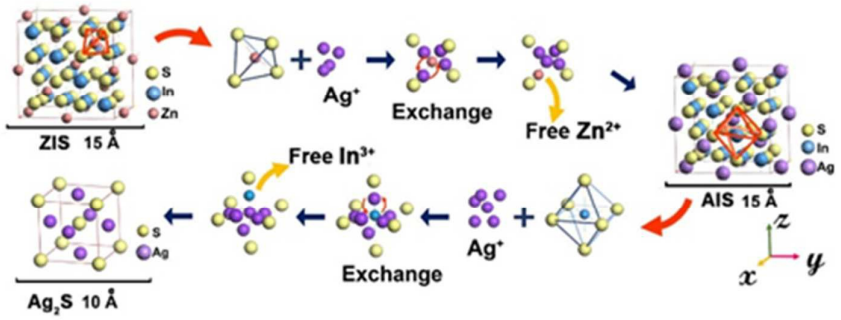

appears as the thickness of AIS. As is shown in Table 3, the thickness of AIS composition increased with Ag content undoubtedly.

On the basis of the XPS analysis and XRD studies above, a summary for the cation change mechanism of ZIS to AIS and AIS to Ag_2S in aqueous solution is illustrated in Scheme 1. Upon adding Ag precursor, Ag^+ cations enter into the lattice of ZIS as interstitials and diffuse around Zn^{2+} and In^{3+}. Among cubic ZIS lattice, Zn^{2+} ions own more binding S^{2-} ions than Zn^{2+} ions. So under the same concentration of Ag^+, Zn^{2+} is comparatively more easily electrostatically perturbed by Ag^+ than In^{3+}. From the point of the electromagnetism, owing to the same order of magnitudes between electrostatic energy of Ag^+ (uniform charge density model: $W = \frac{q^2}{4\pi\varepsilon_0 R}$, where W is the energy, ε_0, q and R is vacuum permittivity, the charge and radius of the cation, respectively) and interaction energy of Zn-S bond ($E = \frac{Q_1 Q_2}{4\pi\varepsilon_0 r}$, where E is the interaction energy, Q_1 and Q_2 is the charge of the two particle, respectively, and r is the distance between the two particles), Ag^+ have a certain probability to break the equilibration of between Zn and S, and thus surround Zn^{2+}. When the amount of Ag^+ reaches the critical concentration, there are enough Ag^+ around, Zn^{2+} in the center of its regular tetrahedron cell is just like a "screened" ion and leave the initial site, and then one of the Ag^+ cation occupies the pristine site of Zn^{2+}. On the other hand, Ag has a larger electronegativity value (1.93) than Zn (1.65) and In (1.78)[31], which mean that Ag is more likely bind with S so that the energy of the overall crystal system decreased to a more stable state. As a comprehensive consequence, cation exchange between Ag^+ and Zn^{2+} happens. Because of the concentration gradient, Zn^{2+} move out of the crystals and bond to methanol finally. Thus, a cubic AIS phase is acquired. With the propagation of the reaction front and the migration of Ag^+ under the condition of heating, the numbers of Ag^+ around In^{3+} increased till they are sufficient to smash the constraint of S^{2-} in the regular octahedron and exchange with In^{3+}. Because of the high mobility, Ag^+ in the tetrahedron rearrange to establish structural equilibrium and Ag_2S with body-centered cubic unit cell is secured. In short, there are two stage during the cation exchange, that is (i) incorporation and diffusion of guest cations (which is analogous to doping), and (ii) bonds disrupting along with *in situ* exchange, which is affected by mobility and concentration, respectively. This mechanism not only elucidates the generation of Ag_2S in the out layers of ZIS without heating, but also explains the more difficult and slow reverse exchange reaction between CdS and Ag_2S.[23]

In the experimental process, methanol and In^{3+} were both introduced to facilitate the generation of AIS contents and reduce the Ag_2S, due to the stronger bond between methanol and binary cation which favor the reaction.[39] According to the proposed mechanism, we designed a new approach to control the exchange rate and progress, and by this, floriated AIS MSs and Ag_2S MSs starting from ZIS MSS were obtained. (Supporting information Figure S4). These results demonstrate a fundamental feature of cation exchange in ternary crystals that both the mobility and the concentration of cation can remarkably tailor the composition and their distribution of product. The work provides a model description of the transformation between different ternary crystals and the convertion from ternary to binary crystals, suggesting that cation exchange is a versatile protocol which can be applied at both nano- and micro-scale.

3.4 UV-vis-NIR aborption and band structure

Diffuse reflectance spectra were used for characterizing the optical properties of materials. As shown in Figure 6, a steep absorption edge for ZIS MSs at around 525 nm is observed,

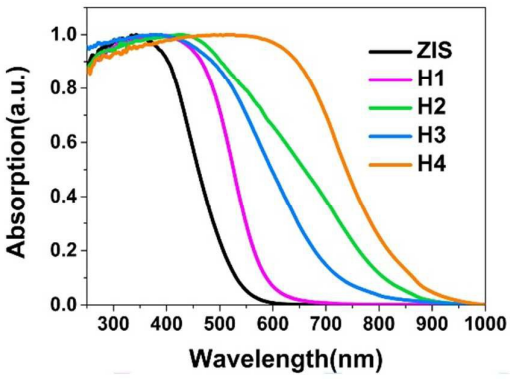

Figure 6. UV-vis-NIR diffuse reflectance absorption spectra of each samples.

Scheme 2. Proposed photocatalytic mechanism for the visible light-driven photocatalytic reaction of dye degradation

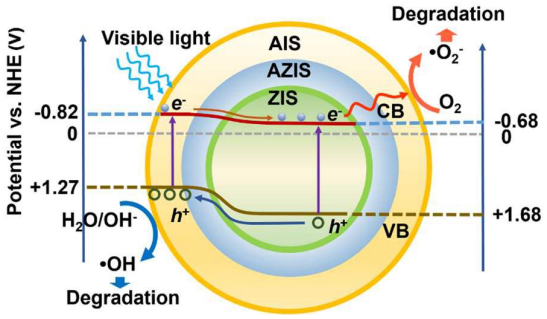

manifesting an intrinsic state-related transition that from valence band (VB) to conduction band (CB). The curves of ZIS/AIS MSs similarly showing the absorption of exciton with red shifts of the absorption onset from 593 to 810 nm, corresponding to the band gap of 2.09 to 1.53 eV (Table 4). This demonstrates the narrowing of the band gap because of the incorporation of Ag into the valence band of AIS.[40-42]

In order to elucidate the charge separation process of the as-prepared ZIS/AIS HMSs, the positions of the bands for ZIS can be calculated using Mulliken electronegativity and band gap values by following equations[43]:

$$E_{VB} = \chi - E^e + 0.5E_g \quad (1)$$

$$E_{CB} = E_{VB} - E_g \quad (2)$$

where E_{VB} and E_{CB} are the valence and conduction band edge potential, respectively; χ is the electronegativity of $ZnIn_2S_4$ (5.00 eV)[44] or $AgIn_5S_8$ (4.72 eV)[34], which is the geometric mean of the electronegativity of the constituent atoms, E^e (~4.5 eV) is the energy of free electrons on the hydrogen scale, and E_g is the calculated band gap (Table 4). Thus, the VB and CB potentials are about +1.68 and –0.68 V for ZIS, and +1.27 and –0.82 V for AIS, respectively. Based on the structure discussed above, a possible mechanism for the degradation of dye is proposed as shown in Scheme 2.

Under visible light illumination, electrons are excited to the CB of AIS, and inject into the CB of ZIS since the E_{CB} is lower than AIS. Simultaneously, the photogenerated holes are injected to the VB of AIS, and directly oxidize OH^- or H_2O molecules because the E_{VB} is more positive than $E_0(O_2/H_2O)$(+1.23 V vs. NHE), so that •OH active species are formed. In the meantime, the photogenerated electrons can migrate to the CB of ZIS and reduce O_2 to produce superoxygen radical ($•O_2^-$) for its more negative potential than $•O_2^-/O_2$ (–0.33 V vs. NHE). Subsequently, some of the $•O_2^-$ continue to react with H^+ to produce H_2O_2, which can also degrade dye. Because of the wide absorption in visible light region than ZIS and the perfect separation of photogenerated carriers, ZIS/AIS HMSs can provide a pronounced degradation efficiency. From the perspective of energy level matching and electrochemistry, this kind of band structure also can be used as light absorbers to fabricate solar cells or hydrogen evolution.

3.5 BET analysis and photocatalystic dye degradation

It is of great importance to evaluate the surface properties of our prepared ZIS/AIS HMSs before applying them to the degradation of dye. Nitrogen adsorption-desorption results shown in Figure 7a demonstrate a type IV isotherm with H3 hysteresis loop in a relatively lower pressure region, suggesting the mesoporous nature of the samples.[11] The broad hysteresis loop illustrates a wide pore size distribution of the ZIS MSs and ZIS/AIS HMSs. Figure 7b shows the pore size distribution graphs of the samples with an average size around 3 nm (Table 4), consist with the SEM characterization.

We chose Rhodamine B (RhB) as a representative cationic dye for the photodegadation test. During the establishment of adsorption/desorption equilibrium, RhB molecules were bond to the surface of ZIS MSs and ZIS/AIS HMSs *via* $–N(Et)_2$ groups, for that positive charged RhB molecules have a strong interaction with ZIS MSs and ZIS/AIS HMSs which have many negative charged S sites.[11] In the process of photodegradation, however, ZIS/AIS HMSs exhibited a higher degradation rate (up to 99.2% for sample H2) than that of ZIS MSs (52.2%) as shown in Figure 7f, although they possess a smaller surface area than that of ZIS MSs (Table 4). The slight blue shifts of the absorption peaks may be the N-de-ethylated intermediates formed in a stepwise manner during the photodegradation.[12] Because of the thinner layers of AIS than the wavelength of visible, visible light with various wavelength can be well absorbed by Ag-In-S, Ag-Zn-In-S and Zn-In-S section, and a marvelous degradation rate is achieved. Further XRD measurement of the ZIS/AIS HMSs before and after 10 times photodegradation cycles shows essentially similar pattern, manifesting a considerable photostability of the HMSs (shown in Supporting information Figure

Table 4. Textural Analysis of ZIS MSs and ZIS/AIS HMSs

sample	absorption edge (nm)	band gap (eV)	BET specific surface area (m^2/g)	pore size (nm)
ZIS	525	2.36	109.16	3.1
H1	593	2.09	103.83	3.0
H2	685	1.81	99.74	3.2
H3	763	1.62	95.23	3.1
H4	810	1.53	92.06	3.0

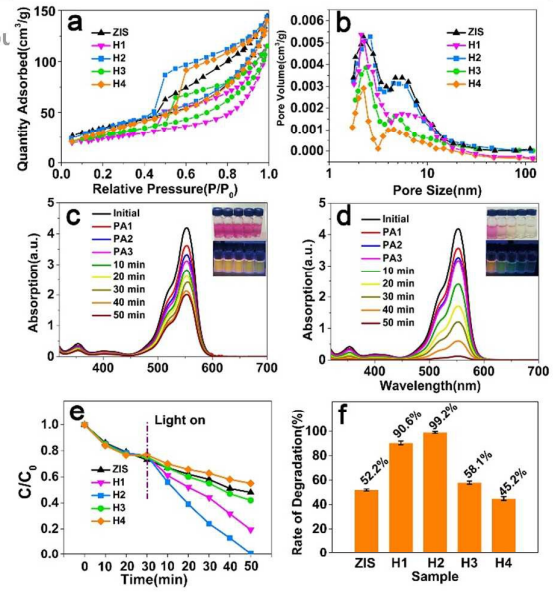

Figure 7. (a) Nitrogen adsorption-desorption isotherms and (b) the pore size distribution plots of ZIS and ZIS/AIS samples; Temporal UV–vis absorption spectra of pre-adsorption (PA) and during the photocatalytic degradation of Rhodamine B in aqueous (c) ZIS MSs and (d)ZIS/AIS HMSs (sample H2) suspension.(Insets: photographs of Rhodamine B solution taken from 10 to 50 min during irradiation); (e) Visible light photocatalytic activities of Rhodamine B and (f) degradation rate after irradiation for ZIS and ZIS/AIS samples.

S5).

Intriguingly, the degradation rate of sample H3 and H4 is lower than H1 and H2, even bellow ZIS MSs for H4. This may be the result of the continuous incorporation of Ag^+ ion. Since the VB of AIS is composed of S 3p and Ag 4d,[40,42,45-47] the continuously increased Ag content (Figure 3j) may lift the VB potential until $E_0(O_2/H_2O)$, thus •OH active species cannot be formed. What's more, with the progressing of reaction and thickening of AIS composition, the length of migration path for both photogenerated carriers extended correspondingly, increasing the recombination probability and therefore reduced the number of active species. So, in the light of the results of photodegradation and XPS analysis, a conclusion could be made that a proper thickness (about 50 nm) of AIS can obviously enhance the rate of degradation, too thin or too thick may result in the deduction of efficiency of photodegradation. This structure may also be used as light absorbers to fabricate solar cells.

4. CONCLUSION

In conclusion, AIS/ZIS HMSs with different composition and band gap were synthesized by cation exchange. Based on the SEM, TEM, XRD and XPS analysis, a possible mechanism for cation exchange about ternary crystals and between ternary to binary crystals was proposed. According to the UV-vis-NIR absorption spectra, the enhanced photodegradation mechanism was discussed, revealing that a proper thickness of AIS composition can in favor of the generation of active species. Furthermore, the photodegradation test of dye was performed, and the ZIS/AIS HMSs demonstrated a marvelous degradation rate up to 99% under the irradiation of visible light. Our work is not only useful in the synthesis of heteromaterial between different band structures but also provide some insight into the design for tailoring the multi-composite with high photocatalystic performance, which may open new opportunities for the evolution of hydrogen and photovoltaic application.

Acknowledgements

We are sincerely grateful to Mr. Jufeng Huang, Dr. Weijia Shao, Prof. Ming Gong, and Dr. Jie Tian for the helpful discussions and technical assistance. We also appreciate Mr. Ali Asad for his useful suggestion in the revised paper. This study is financial supported by the National Natural Science Foundation of China (No. 51272246) and Scientific and Technological Research Foundation of Anhui (No. 12010202035).

REFERENCES

1 Z. Feng, P. Dai, X. Ma, J. Zhan and Z. Lin, *Applied Physics Letters*, 2010, 96, 013104.
2 Y. Sheng, X. Tang and J. Xue, *Journal of Materials Chemistry*, 2012, 22, 1290-1296.
3 J. Song, T. Jiang, T. Guo, L. Liu, H. Wang, T. Xia, W. Zhang, X. Ye, M. Yang, L. Zhu, R. Xia and X. Xu, *Inorganic Chemistry*, 2015, 54, 1627-1633.
4 W. Xiang, C. Xie, J. Wang, J. Zhong, X. Liang, H. Yang, L. Luo and Z. Chen, *Journal of Alloys and Compounds*, 2014, 588, 114-121.
5 T. Torimoto, T. Adachi, K.-i. Okazaki, M. Sakuraoka, T. Shibayama, B. Ohtani, A. Kudo and S. Kuwabata, *Journal of the American Chemical Society*, 2007, 129, 12388-12389.
6 B. Mao, C.-H. Chuang, F. Lu, L. Sang, J. Zhu and C. Burda, *The Journal of Physical Chemistry C*, 2013, 117, 648-656.
7 K. J. Hong, J. W. Jeong, T. S. Jeong, C. J. Youn, W. S. Lee, J. S. Park and D. C. Shin, *Journal of Physics and Chemistry of Solids*, 2003, 64, 1119-1124.
8 S. P. Hong, H. K. Park, J. H. Oh, H. Yang and Y. R. Do, *Journal of Materials Chemistry*, 2012, 22, 18939-18949.
9 S. Shionoya and Y. Tamoto, *J. Phys. Soc. Jpn.*, 1964, 19, 1142-1149.
10 B. Chai, T. Peng, P. Zeng, X. Zhang and X. Liu, *The Journal of Physical Chemistry C*, 2011, 115, 6149-6155.
11 .Y. Chen, R. Huang, D. Chen, Y. Wang, W. Liu, X. Li and Z. Li, *ACS Applied Materials & Interfaces*, 2012, 4, 2273-2279.
12 Z. Chen, D. Li, W. Zhang, Y. Shao, T. Chen, M. Sun and X. Fu, *The Journal of Physical Chemistry C*, 2009, 113, 4433-4440.
13 F. Fang, L. Chen, Y.-B. Chen and L.-M. Wu, *The Journal of Physical Chemistry C*, 2010, 114, 2393-2397.
14 X. Gou, F. Cheng, Y. Shi, L. Zhang, S. Peng, J. Chen and P. Shen, *Journal of the American Chemical Society*, 2006, 128, 7222-7229.
15 T. Jiang, J. Song, H. Wang, X. Ye, H. Wang, W. Zhang, M. Yang, R. Xia, L. Zhu and X. Xu, *Journal of Materials Chemistry B*, 2015, 3, 2402-2410.
16 Y. Yu, G. Chen, G. Wang and Z. Lv, *Int. J. Hydrogen Energy*, 2013, 38, 1278-1285.

17 X. Yuan, R. Ma, W. Zhang, J. Hua, X. Meng, X. Zhong, J. Zhang, J. Zhao and H. Li, *ACS Applied Materials & Interfaces*, 2015, 7, 8659-8666.
18 W. Zhang, Q. Lou, W. Ji, J. Zhao and X. Zhong, *Chemistry of Materials*, 2014, 26, 1204-1212.
19 K.-W. Cheng and S.-C. Wang, *Materials Chemistry and Physics*, 2009, 115, 14-20.
20 Q. A. Akkerman, A. Genovese, C. George, M. Prato, I. Moreels, A. Casu, S. Marras, A. Curcio, A. Scarpellini and T. Pellegrino, *ACS nano*, 2015, 9, 521-531.
21 B. J. Beberwyck, Y. Surendranath and A. P. Alivisatos, *The Journal of Physical Chemistry C*, 2013, 117, 19759-19770.
22 E. Groeneveld, L. Witteman, M. Lefferts, X. Ke, S. Bals, G. Van Tendeloo and C. de Mello Donega, *ACS Nano*, 2013, 7, 7913-7930.
23 R. Gui, J. Sun, D. Liu, Y. Wang and H. Jin, *Dalton Transactions*, 2014, 43, 16690-16697.
24 M. V. Kovalenko, L. Manna, A. Cabot, Z. Hens, D. V. Talapin, C. R. Kagan, V. I. Klimov, A. L. Rogach, P. Reiss, D. J. Milliron, P. Guyot-Sionnnest, G. Konstantatos, W. J. Parak, T. Hyeon, B. A. Korgel, C. B. Murray and W. Heiss, *ACS Nano*, 2015, 9, 1012-1057.
25 J. B. Rivest and P. K. Jain, *Chemical Society Reviews*, 2013, 42, 89-96.
26 W. van der Stam, A. C. Berends, F. T. Rabouw, T. Willhammar, X. Ke, J. D. Meeldijk, S. Bals and C. de Mello Donega, *Chemistry of Materials*, 2015, 27, 621-628.
27 K. Miszta, D. Dorfs, A. Genovese, M. R. Kim and L. Manna, *ACS Nano*, 2011, 5, 7176-7183.
28 D. H. Son, S. M. Hughes, Y. Yin and A. Paul Alivisatos, *Science*, 2004, 306, 1009-1012.
29 J. Park and S.-W. Kim, *Journal of Materials Chemistry*, 2011, 21, 3745-3750.
30 M. D. Regulacio, K. Y. Win, S. L. Lo, S.-Y. Zhang, X. Zhang, S. Wang, M.-Y. Han and Y. Zheng, *Nanoscale*, 2013, 5, 2322-2327.
31 J. Dean, *MATERIAL AND MANUFACTURING PROCESS*, 1990, 5, 687-688.
32 M. A. Hamilton, A. C. Barnes, W. S. Howells and H. E. Fischer, *J. Phys.: Condens. Matter*, 2001, 13, 2425.
33 W. Jost, *The Journal of Chemical Physics*, 1933, 1, 466-475.
34 K. Li, B. Chai, T. Peng, J. Mao and L. Zan, *ACS Catalysis*, 2013, 3, 170-177.
35 T. Ogawa, T. Kuzuya, Y. Hamanaka and K. Sumiyama, *Journal of materials chemistry*, 2010, 20, 2226-2231.
36 Y. Du, B. Xu, T. Fu, M. Cai, F. Li, Y. Zhang and Q. Wang, *Journal of the American Chemical Society*, 2010, 132, 1470-1471.
37 H. Okazaki, *J. Phys. Soc. Jpn.*, 1967, 23, 355-360.
38 D. Shaw, *J. Cryst. Growth*, 1988, 86, 778-796.
39 R. Klenk, J. Klaer, R. Scheer, M. C. Lux-Steiner, I. Luck, N. Meyer and U. Rühle, *Thin Solid Films*, 2005, 480–481, 509-514.
40 M. Dai, S. Ogawa, T. Kameyama, K.-i. Okazaki, A. Kudo, S. Kuwabata, Y. Tsuboi and T. Torimoto, *Journal of Materials Chemistry*, 2012, 22, 12851-12858.
41 M.-l. Dai, K.-i. Okazaki, A. Kudo, S. Kuwabata and T. Torimoto, *Electrochemistry*, 2011, 790-792.
42 W. Xiang, C. Xie, J. Wang, J. Zhong, X. Liang, H. Yang, L. Luo and Z. Chen, *Journal of Alloys and Compounds*, 2014, 588, 114-121.
43 B. Luo, D. Xu, D. Li, G. Wu, M. Wu, W. D. Shi and M. Chen, *ACS Applied Materials & Interfaces*, 2015, DOI: 10.1021/acsami.5b03535.
44 Y. Xu and M. A. Schoonen, *Am. Mineral.*, 2000, 85, 543-556.
45 I. Tsuji, H. Kato, H. Kobayashi and A. Kudo, *Journal of the American Chemical Society*, 2004, 126, 13406-13413.
46 I. Tsuji, H. Kato and A. Kudo, *Angewandte Chemie*, 2005, 117, 3631-3634.
47 I. Tsuji, H. Kato and A. Kudo, *Chemistry of Materials*, 2006, 18, 1969-1975.

TOC

Here we report a new protocol of synthesizing $ZnIn_2S_4/AgIn_5S_8$ heteromicrospheres with excellent photodegradation rate *via* partial cation exchange.